Acta Cryst. (1996). B**52**, 780–789

Incommensurate Modulated Disorder in $Ba_{0.85}Ca_{2.15}In_6O_{12}$

G. BALDINOZZI,[a] F. GOUTENOIRE,[a] M. HERVIEU,[a] E. SUARD[b] AND D. GREBILLE[a]*

[a]*Laboratoire CRISMAT, URA CNRS 1318, ISMRa, Boulevard Juin, F14050 Caen CEDEX, France, and* [b]*Institut Laüe Langevin, BP156, Avenue des Martyrs, F38042 Grenoble CEDEX, France. E-mail: dom@crcrisu.ismra.fr*

(*Received 27 February 1996; accepted 15 May 1996*)

Abstract

The tunnel structure of the oxide $Ba_{0.85}Ca_{2.15}In_6O_{12}$ has been revisited. A mono-incommensurate modulation has been evidenced by electron diffraction. The simultaneous refinement of X-ray and neutron powder diffraction patterns has allowed a complete determination of the incommensurate structure [$P3(\frac{1}{3}\frac{1}{3}\gamma)$]. The existence of a modulated disorder, affecting Ba and Ca atoms, has been pointed out. The occupancy modulation concerning Ba and Ca atoms located on the hexagonal tunnel axis induces a modulation of the Ba—O bond lengths. The high-resolution electron microscopy study has shown the existence of twinning domains and of crystal regions possessing a defective arrangement of the modulation.

1. Introduction

The structures of compounds belonging to the family $AA'_2M_6O_{12}$ (A and A' being alkaline-earth elements and M being In or Tl) present both chemically and structurally interesting features. These compounds are a generalization of the AMO_4 family, which presents a framework built up from multiple rutile ribbons. Some examples of these structures have been recently illustrated by the synthesis of new thallates (Michel, Hervieu, Caignaert & Raveau, 1992; Goutenoire, Caignaert, Hervieu, Michel & Raveau, 1995*a*,*b*). Two of them, $SrTl_2O_4$ and $CaTl_2O_4$ (Goutenoire *et al.* 1995*a*,*b*), are built up from double rutile ribbons forming a MO_2 framework, but they differ by the way these strings of double octahedra are connected: $CaTl_2O_4$ (Goutenoire *et al.* 1995*a*) is isotypic to $CaTi_2O_4$ (Bertaut, Blum & Magnano, 1956), whereas $SrTl_2O_4$ is isotypic to $CaFe_2O_4$ (Hill, Peiser & Rait, 1956). The indium-based oxides $CaIn_2O_4$ (Cruickshank, 1964) and $SrIn_2O_4$ (Schenck & Müller-Buschbaum, 1973) are both isotypic to $CaFe_2O_4$.

The size of the ions located in the framework interstices assumes considerable importance for the way in which the ribbons are joined, *i.e.* for the size and shape of the tunnels. When Ba is introduced in a MO_2 framework large tunnels are formed, bordered by three double ribbons. These rutile ribbons leave hexagonal tunnels and prismatic voids where the remaining cations are located. These oxides, with the general chemical formula $AA'_2M_6O_{12}$, are interesting because of the varied physical properties associated with the structure. Small variations in the stoichiometry and/or selected cationic substitutions may produce the onset of ionic conduction properties. These structures may also be good candidates as encapsulants as big cations may be trapped in tunnels. This family of compounds presents some similarities with the hollandite-type structures where similar phenomena occur. This paper focuses on one of the members of this system: $BaCa_2In_6O_{12}$.

Single crystals of $BaCa_2In_6O_{12}$ were first synthesized and characterized by Lalla & Müller-Buschbaum (1988) by the usual X-ray diffraction techniques. The structure resolution was carried out in the $P6_3/m$ space group. To describe the structure in this space group, it is necessary to introduce a statistical disorder for Ba atoms located on the hexagonal tunnel axis.

In the present paper the investigation is carried out by electron microscopy and X-ray and neutron powder diffraction. Evidence of the existence of incommensurate superstructural reflections is given and it is proved that even if the basic structure seems to be quite simple, the actual crystal structure is more complex. The incommensurate modulated structure is determined by the simultaneous refinement of X-ray and neutron powder diffraction data using the Rietveld method.

2. Experimental

2.1. *Sample synthesis*

Powdered samples of $BaCa_2In_6O_{12}$ were obtained, starting from high purity amounts of BaO_2, CaO and In_2O_3. The mixture product was grounded, pressed into pellets, placed into alumina crucibles and finally heated at 1600 K overnight under room atmosphere. The sintered specimen was pale brown. Preliminary tests of powder quality (with parasitic phases and reflection profiles) were performed on a Seifert standard X-ray diffractometer using Cu $K\alpha_1$ radiation. This analysis confirmed the good crystallization of the samples. The stoichiometry was checked through energy dispersive X-ray spectroscopy (EDX or EDS) analysis. The powder samples are homogeneous and a slight deficiency of Ba contents was detected. The average chemical formula of the compound is $Ba_{0.85}Ca_{2.15}In_6O_{12}$.

Table 1. *Experimental data of* $Ba_{0.85}Ca_{2.15}In_6O_{12}$

Space group	$P3(\frac{1}{3}\frac{1}{3}\gamma)$	
a (Å)	9.8880 (1)	
c (Å)	3.2170 (1)	
V (Å^3)	272.4	
Modulation vector	$\frac{1}{3}\mathbf{a}^* + \frac{1}{3}\mathbf{b}^* + 0.1385(1)\mathbf{c}^*$	
Formula weight	1083.82	
Z	1	
D_x (g cm^{-3})	5.44	
	X-ray	Neutron
Wavelength (Å)	1.392218	1.2765 (1)
Monochromator	Graphite	
Step scan width (2θ,°)	Variable (0.02–0.10)	0.05
2θ range (°)	8.0–138.0	7.1–158.0

2.2. *Electron microscopy*

Electron microscopy was performed on a JEOL 200CX equipped with an eucentric goniometer sample holder (± 60°). HREM was performed on a TOPCON 2B electron microscope operating at 200 kV (0.4 mm). All patterns were recorded at room temperature.

2.3. *X-ray and neutron scattering*

The neutron powder diffraction pattern was collected on the D2b diffractometer at ILL in Grenoble. The powder sample was loaded in a vanadium canister. Data collection was performed using 0.12765 nm wavelength up to $\sin\theta_{max}/\lambda$ of 7.7 nm^{-1} at room temperature.*

The X-ray powder diffraction pattern was recorded on a prototype two-axis diffractometer equipped with a 18 kW rotating anode in Laboratoire de Chimie-Physique du Solide (URA CNRS 453) at Ecole Centrale de Paris. Graphite-monochromatized Cu $K\beta$ radiation was employed for data collection in order to span a larger zone of the Ewald sphere. Measurements were performed at room temperature up to $\sin\theta_{max}/\lambda$ of 6.7 nm^{-1}. The neutron scattering lengths used in the structure refinement were 5.06, 4.90, 4.065 and 5.803 for Ba, Ca, In and O, respectively (Wilson, 1992).

The powder diffraction patterns were refined by the Rietveld program *XND* (Version 1.10) written by Bérar (1992). This program allows the simultaneous refinement of X-ray and neutron diffraction patterns and it has been recently modified to allow the treatment of incommensurate phases, using the four-dimensional formalism for superspace symmetry (de Wolff, 1977; de Wolff, Janssen & Janner, 1981). During the early stages of the refinement of the X-ray pattern, we became aware of a slight broadening of the satellite reflections compared with the main ones. As the spectral width presents a fast increase with the scattering angle, this broadening affects only the first few satellites and it was not relevant for the fit of the model. The four-dimensional Fourier series maps were performed using the structure refinement package *JANA*94 (Petříček, 1994). The integrated intensities used as input data were extracted from the powder diffraction pattern using *XND*.

* The numbered intensity of each measured point on the profile has been deposited with the IUCr (Reference: DU0409). Copies may be obtained through The Managing Editor, International Union of Crystallography, 5 Abbey Square, Chester CH1 2HU, England.

3. Results

3.1. *Lattice, symmetry and modulation vectors*

The electron diffraction investigation of numerous crystallites confirmed the homogeneity of the powder sample. The main reflections are compatible with a hexagonal subcell with $a \simeq 9.9$ and $c \simeq 3.2$ Å. The subcell parameters and symmetry are consistent with those proposed by Lalla *et al.* (1988). The [001] electron diffraction pattern is given in Fig. 1.

The electron diffraction patterns along the [100] zone, *i.e.* perpendicular to the hexagonal plane, contain extra spots lying on incommensurate positions, as shown in Fig. 2(*a*). Third-order satellites are commonly observed. Regularly, in [100] zone patterns, four intense satellites are observed; nevertheless, in some pictures, only two

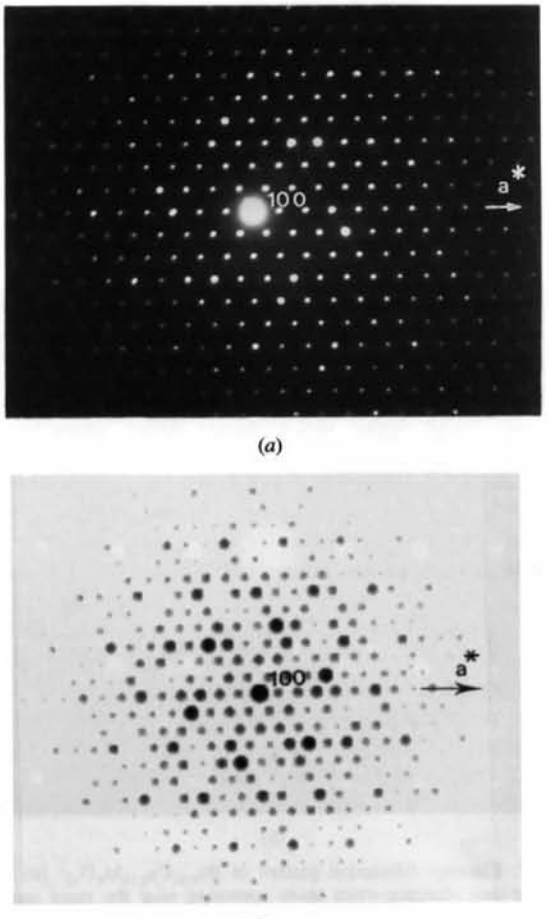

(*a*)

(*b*)

Fig. 1. (*a*) Experimental and (*b*) calculated electron diffraction pattern of $Ba_{0.85}Ca_{2.15}In_6O_{12}$: [001] zone axis.

satellite reflections surrounded the main spots (Fig. 2*b*); this fact can be interpreted as the existence of at least two orientational domains, the (110) plane playing the role of a mirror (see later). In this hypothesis the modulated phase is mono-incommensurate and all order satellites can be indexed by a one-dimensional modulation vector $\mathbf{q} = \frac{1}{3}\mathbf{a}^* + \frac{1}{3}\mathbf{b}^* + \gamma\mathbf{c}^*$.

In such electron diffraction patterns the conditions limiting the reflection are scarcely visible due to multiple diffraction phenomena; by tilting along c^* it clearly appears that $00l$, $l = 2n$.

The accurate analysis of the X-ray and neutron powder diffraction patterns (Figs. 3 and 4) corroborates this first description. The main reflections can be indexed by the hexagonal space group determined by electron microscopy and single-crystal X-ray diffraction (Lalla *et al.*, 1988). The refinement of lattice parameters has been carried out by least-squares using 12 well resolved peaks of the X-ray pattern with $2\theta < 90°$. Lattice parameters at 294 K are $a = b = 0.98880\,(1)$ and $c = 0.32170\,(1)$ nm. These lattice parameters do not allow a complete indexing of all the diffraction peaks on the X-ray and neutron patterns, giving evidence of the existence of weak satellite reflections.

Table 2. *Refinement statistics: average structure*

	X-ray	Neutron
R_{wp}	12.67	7.64
R_{exp}	3.78	2.41
S	3.34	3.15
R_F	4.06	6.38
R_I	5.19	8.01

In order to determine the actual symmetry of the modulated structure we have introduced a modulation vector compatible with the electron diffraction measurements. It should be noticed that the choice of only one modulation vector, $\mathbf{q} = \frac{1}{3}\mathbf{a}^* + \frac{1}{3}\mathbf{b}^* + \gamma\mathbf{c}^*$, is not compatible with a four-dimensional hexagonal Bravais class for mono-incommensurate structures and is only compatible with the trigonal class $\bar{3}1mP(\frac{1}{3}\frac{1}{3}\gamma)$.

As no evidence of the systematic absence of satellite reflections can be remarked on the electron microscopy

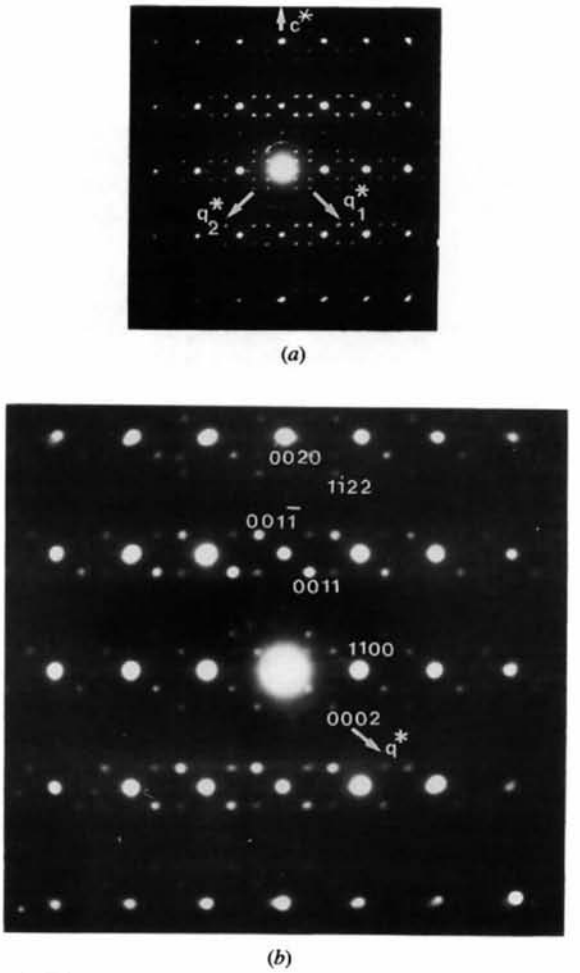

Fig. 2. Electron diffraction pattern of $Ba_{0.85}Ca_{2.15}In_6O_{12}$: (*a*) [100] zone axis showing extra spots appearing near the main spots of the hexagonal lattice. (*b*) In this image, relative to the same zone axis, only two incommensurate spots surround the main ones. The existence of more than two incommensurate spots is a result of twinning phenomena.

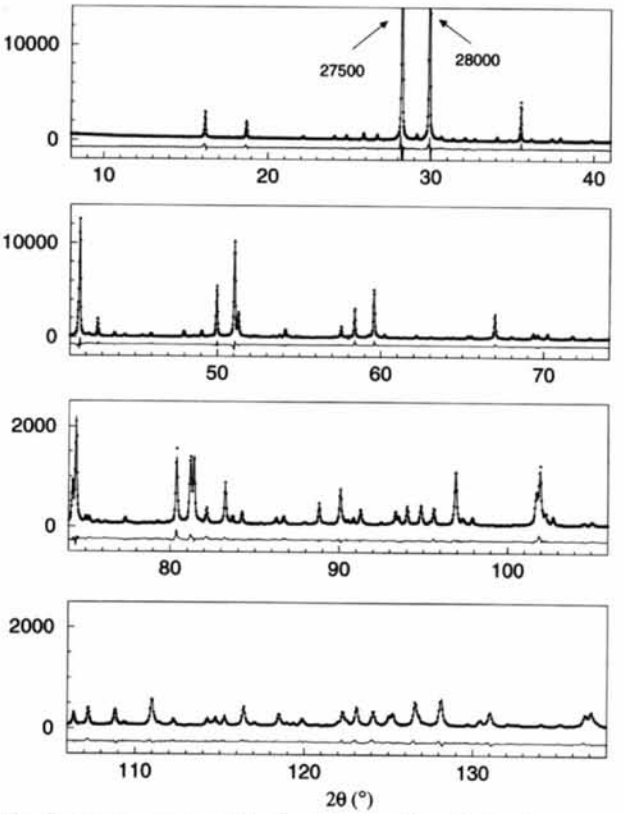

Fig. 3. X-ray powder diffraction pattern. The displayed patterns are observed (black dots), calculated (continuous line) and the difference.

Table 3. *Average positions and anisotropic thermal parameters in the basic structure ($P6_3/m$)*

	x	y	z	P	b_{11}	b_{22}	b_{33}	b_{12}	B_{eq}† or B_{iso}
Ba	0	0	0.160 (12)	0.86 (1)	0.0014 (4)	0.0014 (4)	0.20 (8)	0.0007 (2)	3.1†
Ca	1/3	2/3	1/4	1					0.21 (4)
In	0.3472 (1)	−0.0044 (2)	1/4	1					0.32 (2)
O1	0.1935 (3)	0.3048 (3)	1/4	1	0.0018 (2)	0.0065 (3)	0.0054 (10)	0.0059 (4)	0.39†
O2	0.5316 (3)	0.3985 (2)	1/4	1	0.0021 (2)	0.0003 (2)	0.0131 (11)	0.0002 (3)	0.46†

plates or on the powder diffraction patterns, the only acceptable superspace groups compatible with the previous restrictions are the centrosymmetric superspace group $P\bar{3}(\frac{1}{3}\frac{1}{3}\gamma)$ and the non-centrosymmetric $P3(\frac{1}{3}\frac{1}{3}\gamma)$.

The good resolution of the powder patterns allows a reliable determination of the components of the modulation vector. The $\mathbf{c}^*$ component of the modulation vector is actually incommensurate: $\mathbf{q} = \frac{1}{3}\mathbf{a}^* + \frac{1}{3}\mathbf{b}^* + 0.1385\,(1)\mathbf{c}^*$ at 294 K. This modulation vector allows an accurate description of the d spacings of the incommensurate superstructure and a complete indexing of the powder diffraction patterns.

3.2. *Refinement of the structure*

The refinement of the average structure in the group $P6_3/m$, according to the literature, gives low R factors (Table 2). In the basic structure of $Ba_{0.85}Ca_{2.15}In_6O_{12}$ ($P6_3/m$), Ba atoms sit on the threefold axis [4(e)], Ca atoms on $\bar{6}$ [2(c)], In atoms on mirror planes at $z = \frac{1}{4}$ and $z = \frac{3}{4}$ [6(h)]. The results of the refinement are presented in Table 3. The orthogonal projection of the average structure along the **c** axis is presented in Fig. 5.

The structure can be described as double edge-sharing rutile chains consisting of InO_6 octahedra forming hexagonal tunnels along [001]. Ba atoms are distributed in rows along these hexagonal tunnels, while Ca atoms are located in the prismatical voids left by the octahedra (Fig. 5). In each cell Ba atoms occupy statistically only one of the four sites.

It is worth noting that, in addition to the occupational disorder concerning Ba atoms, their thermal ellipsoids are strongly elongated along the tunnel axis. Actually, the value of b_{33} produces an almost continuous distribution of electronic density along the tunnel axis.

In the description of the modulated structure of $Ba_{0.85}Ca_{2.15}In_6O_{12}$, the coordinates of each atom μ can be specified as a Fourier expansion of the internal coordinate: $\bar{x}_4^\mu = \mathbf{q} \cdot \bar{\mathbf{x}}^\mu$, where $\bar{\mathbf{x}}^\mu$ is the average position of the considered atom. The complete structure of $Ba_{0.85}Ca_{2.15}In_6O_{12}$ involves both displacive and occupational modulations. The coefficients of the Fourier expansion of the modulation functions are used as independent parameters in the refinements: the position for the atom μ in the modulated structure along the coordinate i is given by

$$u_i^\mu(\bar{x}_4^\mu) = B_{0i}^\mu + \sum_{n=1}^{\infty}[A_{in}^\mu \sin(2\pi n\bar{x}_4^\mu) + B_{in}^\mu \cos(2\pi n\bar{x}_4^\mu)].$$

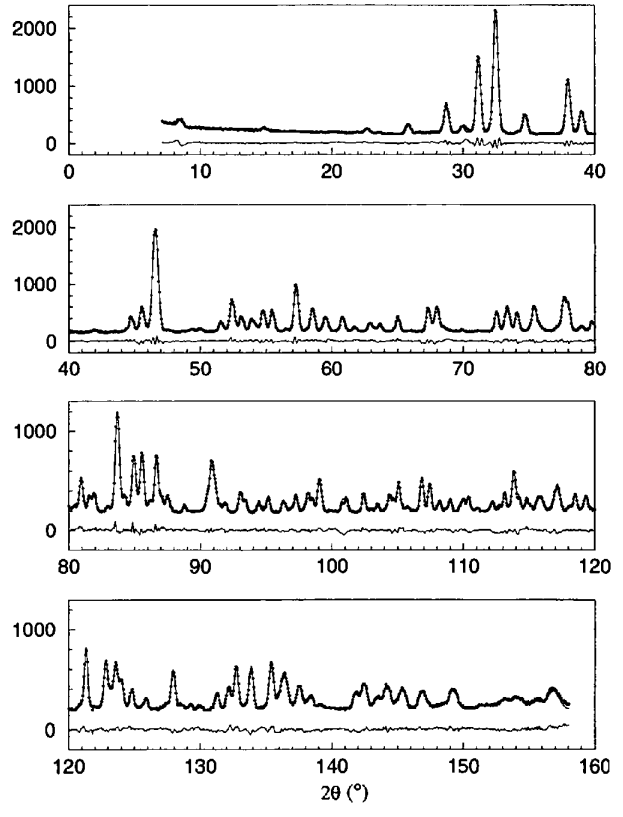

Fig. 4. Neutron powder diffraction patterns. The displayed patterns are observed (black dots), calculated (continuous line) and the difference.

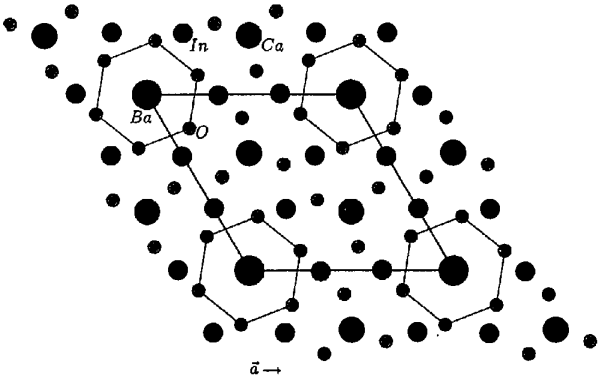

Fig. 5. Orthogonal projection of the hexagonal plane of $Ba_{0.85}Ca_{2.15}In_6O_{12}$ in the average structure.

For the occupational modulation

$$P^{\mu}(\bar{x}_4^{\mu}) = D_0^{\mu} + \sum_{n=1}^{\infty}[C_n^{\mu}\sin(2\pi n\bar{x}_4^{\mu}) + D_n^{\mu}\cos(2\pi n\bar{x}_4^{\mu})].$$

The restrictions imposed by the site symmetries of the considered Wyckoff positions on the Fourier terms of the atomic modulation functions were found solving the de Wolff equations (de Wolff, 1977; de Wolff *et al.*, 1981).

The occupational modulation is restricted, as will be shown later in this section, to the atoms located in the hexagonal tunnel (*i.e.* Ba) with a possible substitution with Ca. Since only first- and second-order satellites are observed, the refinement parameters included only Fourier amplitudes of the first and second order.

We have underlined in the structural study of the average structure the large thermal displacements affecting Ba atoms along the z axis. Moreover, four sites, randomly occupied, were necessary to describe this atom. We can safely suggest that the existence of four Ba sites supports the existence of an occupational modulation for these atoms, while the strong thermal displacement parameter along **c** may be related to the presence of a displacive modulation. We have also remarked that the thermal ellipsoids of all the oxygen atoms are strongly elongated along the **c** direction. This suggests that the main atomic displacements of these atoms take place along this direction.

It is worth remarking that in the centrosymmetric group $P\bar{3}(\frac{1}{3}\frac{1}{3}\gamma)$, stronger restrictions apply to the modulation components. In particular, it is not possible to introduce a modulation for Ba atoms as long as they are at the origin. Moreover, if a z coordinate different from zero is chosen for the average position of Ba atoms, the inversion symmetry will generate an equivalent position at the coordinate $\bar{z}$. Similar considerations hold for the occupancies of the two symmetry-related sites. Therefore, the resulting picture is not very satisfactory and the non-centrosymmetric group $P\bar{3}(\frac{1}{3}\frac{1}{3}\gamma)$ has been chosen for the structural refinement.

It is apparent from the large thermal displacement along the z axis that it is very difficult to define an average position of Ba atoms in the modulated structure; to overcome this problem we have undertaken a careful study of the series of Fourier differences in four-dimensional space. To this purpose, we have refined the X-ray data pattern by the Rietveld method and extracted the integrated intensities of all reflections. These data have been used as input to the program *JANA*94 (Petříček, 1994). The electronic density in the Ba channel is displayed in Fig. 6. Three sites can be outlined on this Fourier map and confirm our option for the non-centrosymmetric space group. One site is at the origin, while the two others sit at *ca* $z = \pm\frac{1}{4}$ along the z axis. It is obvious that these sites are not occupied simultaneously as the maxima occur at different values of the four-dimensional coordinate. Moreover, no displacive modulation seems to affect these sites. This model can explain the distribution of the electronic density of the average model.

The refinement of the structure has been carried out introducing three occupationally modulated Ba sites, Ba1, Ba2 and Ba3, at $z = -\frac{1}{4}$, $z = \frac{1}{4}$ and $z = 0$, respectively. To describe the occupational modulation, Fourier terms up to second order have been considered. The

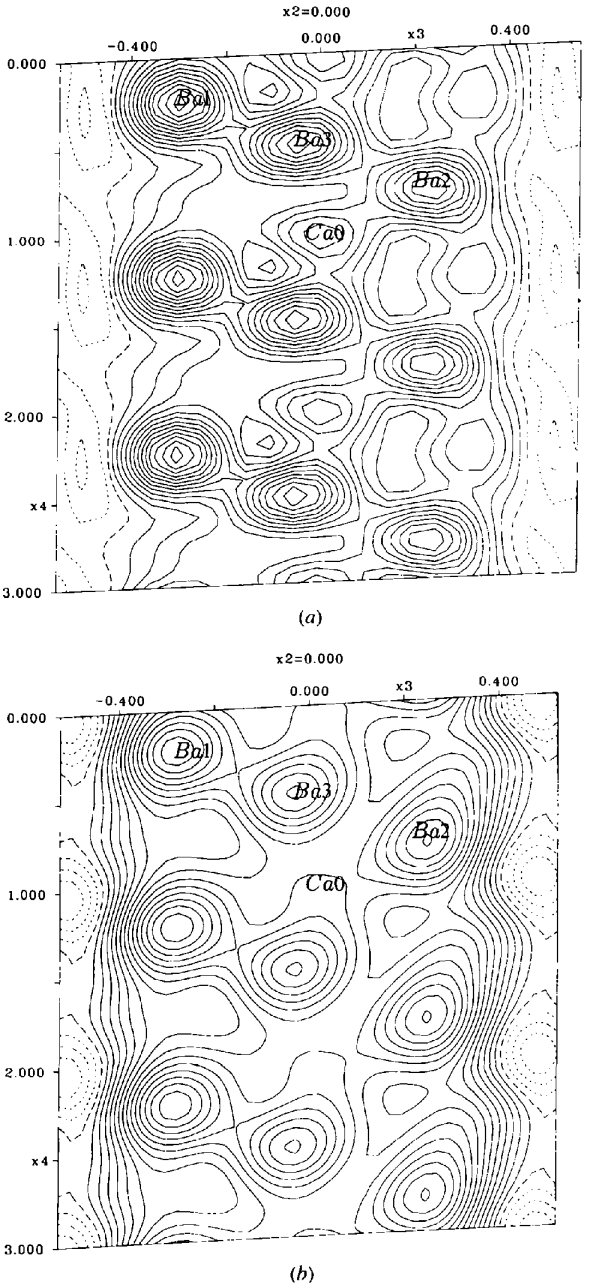

Fig. 6. Difference-Fourier series maps from (*a*) neutron powder diffraction data and (*b*) X-ray powder diffraction data: residual density is obtained omitting Ba atoms from the model.

Table 4. *Refinement statistics: incommensurate refinement*

	X-ray	Neutron
R_{wp}	8.05	4.82
R_{exp}	3.78	2.41
S	2.13	2.00
R_{F0}	3.30	2.79
R_{F1}	7.78	5.99
R_{F2}	9.24	6.09
R_F (overall)	5.00	4.23
R_I (overall)	4.98	5.42

Table 5. *Atomic positions and isotropic thermal parameters in the incommensurate structure*

	x	y	z	B_{iso}
Ba1	0	0	−0.295 (4)	0.35 (7)†
Ba2	0	0	0.222 (7)	0.35 (7)†
Ba3	0	0	−0.064 (5)‡	0.35 (7)†
Ca0	0	0	−0.064 (5)‡	0.35 (7)†
Ca1	1/3	2/3	0.267 (5)	0.46 (3)†
Ca2	2/3	1/3	−0.255 (7)	0.46 (3)†
In1	0.3492 (4)	−0.0005 (4)	1/4	0.39 (2)†
In2	−0.3455 (4)	0.0068 (4)	−0.253 (2)	0.39 (2)†
O1*a*	0.1910 (5)	0.3040 (4)	0.250 (5)	0.24 (3)†
O1*b*	−0.1948 (6)	−0.3024 (6)	−0.241 (4)	0.24 (3)†
O2*a*	0.5293 (6)	0.3970 (6)	0.248 (5)	0.44 (3)†
O2*b*	−0.5331 (6)	−0.3997 (7)	−0.246 (5)	0.44 (3)†

The parameters marked with † or ‡ are constrained.

Table 6. *Occupational modulation parameters for the incommensurate structure*

	D_0	C_1	D_1	C_2	D_2
Ba1	0.35 (3)	0.430 (1)	0.057 (2)	−0.018 (3)	−0.196 (7)
Ba2	0.17 (2)	−0.345 (1)	0.073 (2)	−0.076 (3)	−0.153 (7)
Ba3	0.31 (2)	0	−0.368 (2)	0	0.193 (5)
Ca0	0.10 (2)	0	0.119 (6)	0	0.117 (13)

Table 7. *Displacive modulation parameters for the incommensurate structure*

		A_1	B_1	A_2	B_2
In1	x	0.0053 (1)	0	0	0
	y	0.0061 (1)	0	0	0
	z	0.0006 (1)	0	0	0
In2	x	−0.0030 (1)	0	0	0
	y	0.0018 (1)	0	0	0
	z	0	0.0124 (1)	0	0
O1*a*	x	0.0032 (1)	0	0	0
	y	0.0089 (1)	0	−0.0084 (1)	0
	z	−0.0267 (2)	0	0	0
O1*b*	x	−0.0187 (1)	0	−0.0024 (2)	0
	y	−0.0339 (1)	0	0	0
	z	0.0093 (3)	0	0	0
O2*a*	x	0	−0.0095 (1)	0	0
	y	−0.0020 (1)	0	0	0
	z	0	0	0	0
O2*b*	x	0	0.0061 (1)	0	0
	y	0	0	0	0
	z	−0.0334 (2)	0	0	0

z coordinates of the Ba sites have also been refined and refined modulation terms up to second order were necessary to describe properly the displacements of the O atoms defining the hexagonal tunnel. Only first-order terms were necessary to describe the displacements of the other atoms. The observed and calculated X-ray and neutron diffraction patterns are presented in Figs. 3 and 4.

The final results of the refinement of the modulated structure are summarized in Tables 4–7. These results show that Ba atoms actually occupy three different sites at $z = -0.295\,(4)$, $-0.064\,(5)$ and $0.222\,(7)$, respectively. The calculation of the difference-Fourier density map with the refined description of the Ba sites does not show any significant residual. The resulting incommensurate structure of the hexagonal tunnel is presented in Fig. 7.

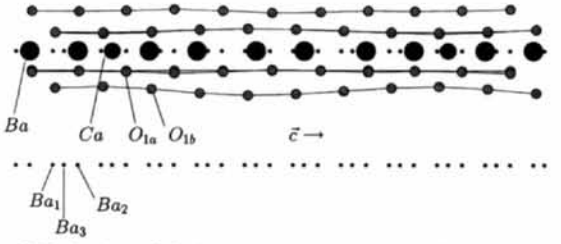

Fig. 7. Projection of the incommensurate structure along [001].

3.3. *High-resolution images*

High-resolution images along the [001] zone axis were recorded for several crystallites; the image contrast consists of one very bright or very dark dot, correlated to the Ba positions, in a hexagonal pattern of bright or dark dots, depending on the focus value. Such an image is given in Fig. 8(*a*), where the positions of the cations appear as bright dots. No local variation nor modulation of the contrast were observed along this direction, in agreement with the previously described symmetry of the average structure.

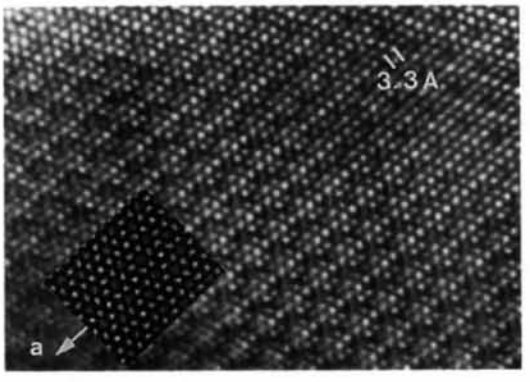

Fig. 8. High-resolution image taken along the [001] zone axis. The inset shows the calculated image for a focus of −500 Å and a crystal thickness of 34 Å.

Simulated images have been calculated with the positional parameters of the average structure given in Table 3, which fit perfectly with experiment. The calculated image for a focus value of −500 Å and a crystal thickness of 34 Å is superimposed on the experimental image in Fig. 8(*a*).

Most of the images were recorded along the [100] direction in order to obtain information on the nature and distribution of the modulated structure. The interpretation of the projected potential along this direction is not straightforward. The analysis of the contrast was carried out in two steps.

First, as will be explained further, there exist in the crystals small areas where the contrast is not modulated. The experimental images recorded for these areas have therefore been firstly interpreted and compared with the simulated images calculated for the positional parameters given in Table 3. Viewing the structure from [110], three types of atomic layers are stacked along [1$\bar{1}$0]: one is built up from Ba and Ca atoms and the two others are two staggered similar rows where Ca and In atoms alternate.

The calculation of a commensurate approximation (3*a*.3*a*.7*c*) of the incommensurate cell involves *ca* 1400 independent atoms. For this reason we were not able to calculate this model. In order to explain the modulation of contrast we observe along [001], we have considered a simplified model involving only two cells (*a*.*a*.2*c* supercell). Two independent and alternatively occupied sites for Ba atoms (Ba1 and Ba2) have been used to calculate the simulated images. One of the easily interpretable typical images is obtained for a focus value close to the Scherzer value (∼ −250 Å), where low electron-density zones are imaged as bright dots. Such an image is presented in Fig. 9(*a*) and compared with the simulated image calculated for a focus value of −250 Å *versus* the crystal thickness (Fig. 9*b*). It appears that the contrast evolves from one row of bright dots and two grey ones (for a thickness of 34 Å) to a single row of bright dots, 3.2 Å spaced. These bright dots are correlated to the positions of the Ca atoms located between two Ba atoms in the first type of layer. The experimental and calculated contrasts fit well. This model explains the variation of contrast observed along [001]: one bright dot out of two is highlighted as soon as the crystal thickness is superior to a few tens of Å, as it is scarcely visible for 68 Å, but clear for 102 Å.

In a second step the modulated areas have been characterized. At the top of Fig. 10, which corresponds to a thin edge of the crystal, the modulation begins to be observed through a variation in contrast of the bright dots, some being highlighted whereas others are darker, but also through the interdot distances, the brighter dots being more spaced than the darker ones. This is in agreement with the occupancy modulation affecting Ba atoms as it gives rise to different interatomic distances between these atoms (Fig. 7). In the bottom part of the image the modulation is clearly visible; the periodicity along [001] is seven times the *c* parameter and three times d_{110} along [110]. However, the observation of a large number of crystallites showed that this arrangement is not so regular within the matrices.

3.4. *Defective arrangement of the modulation*

Two common structural features are observed in Figs. 11(*a*) and (*b*). The first (Fig. 11*a*) shows the existence

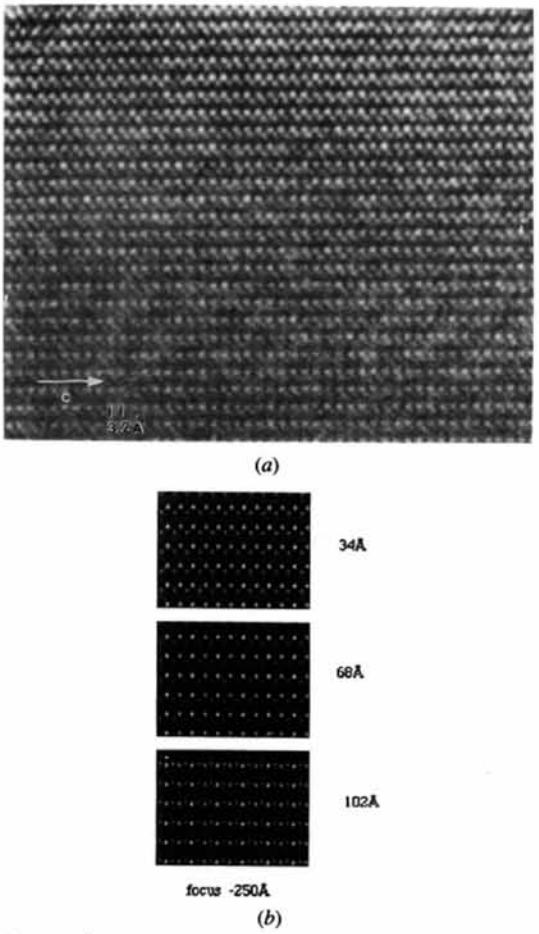

(*a*)

(*b*)

Fig. 9. (*a*) [1$\bar{1}$0] high-resolution image taken in a thin crystal edge. (*b*) Calculated high-resolution images for three different thicknesses.

Fig. 10. High-resolution image, taken along the [1$\bar{1}$0] zone axis, showing a modulation of the sequence of intensities of bright and dark dots.

of oriented modulated domains (see white arrows); the corresponding electron diffraction pattern is that of Fig. 2(*b*). The orientation of the wavevector changes: the (110) plane playing the role of a mirror, but the twin boundary is not straight and wanders in the matrix. The size of such domains is highly variable, from a few nanometers as in that example to several hundred nanometers.

The periodicity of the modulation does not always correspond to the expected one, *i.e.* close to 7*c*. In some parts of the crystal the local periodicity is closer to 6*c* (central part of Fig. 11*b*, where a 3*a*.3*a*.6*c* supercell is drawn) or even 5*c*, retaining the translation $\mathbf{a}+\mathbf{b}$. These different periodicities are not perfectly established over large areas so that the mismatch is absorbed through the formation of antiphase boundaries (APB). One example is shown in Fig. 11(*b*), where the local periodicities are marked by black lines; looking at the image at grazing incidence, it is easy to see the existing translations. At the level of the antiphase boundary, the periodicity is scarcely visible. This disappearance of the modulated contrast is often due to the existence of twin domains or antiphases. A third origin deals with the breaking of the translation $\mathbf{a}+\mathbf{b}$; this can be easily observed in the area marked by curved arrows in Fig. 11(*b*). However, sometimes no evident origins are observed and the existence of small unmodulated areas can be probably correlated to local disordering phenomena along the viewing direction, so that an apparently random distribution of the Ba atoms is observed.

4. Discussion

The most interesting feature of the modulated structure is the occurrence of a modulated distribution of Ba atoms in the hexagonal tunnels. The variations of the Ba—O bond lengths *versus* the four-dimensional coordinate are shown in Fig. 12. To interpret these distances, it is necessary to take into account the modulation of occupancy affecting the three Ba sites. The three sites are not simultaneously occupied: as the maxima of the distribution function are dephased of $\sim\frac{1}{3}$ along the fourth coordinate, with a full width at half-maximum of $\sim\frac{1}{3}$ in each cell, generally only one position is actually occupied. It can be noticed that the Ba—O distances range from 2.3 to ~ 3.4 Å. The lower bond is largely shorter than the sum of the atomic radii of Ba and O and it should not be reached. Actually, if we consider the occupancies of the three sites, we can assume that the short distances are never obtained as the probability of occupying the site is negligible. The three Ba sites present different environments (Fig. 12): Ba1 and Ba2

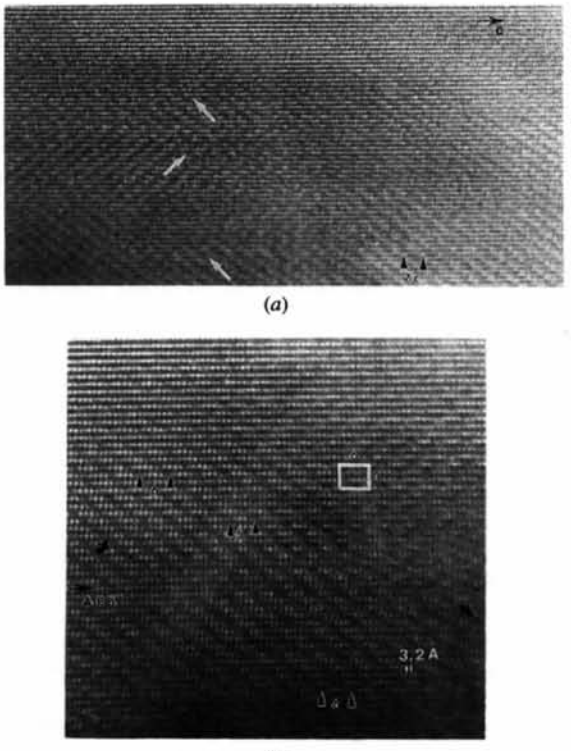

(*a*)

(*b*)

Fig. 11. (*a*) Evidence of twinning domains. (*b*) Image of a crystal exhibiting small regions where the modulation vector is closer to $\frac{1}{3}\mathbf{a}^*+\frac{1}{3}\mathbf{b}^*+\frac{1}{6}\mathbf{c}^*$.

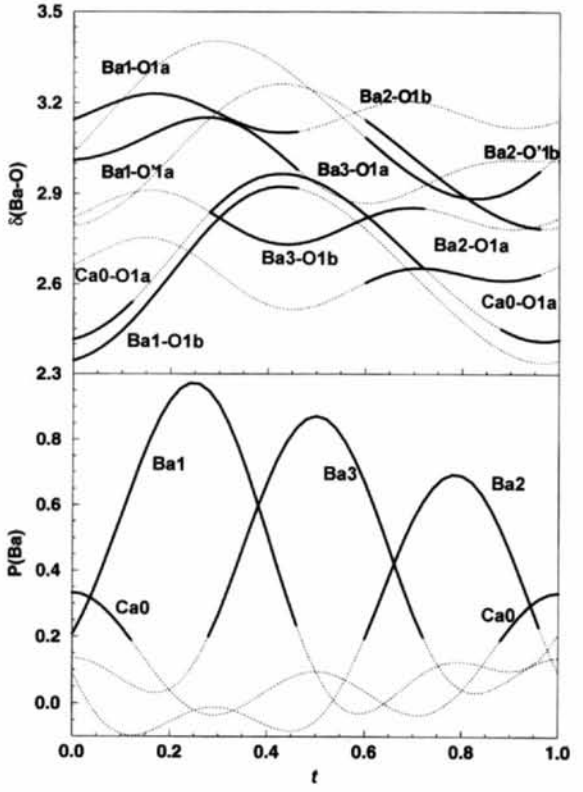

Fig. 12. Ba—O distances and modulation of the occupancies of Ba sites in the hexagonal tunnel.

form three short bonds with the O atoms located at approximately the same z coordinate and six longer bonds with the other O atoms located at *ca* $z \pm \frac{1}{2}$. On the other hand, Ba3 atoms, which occupy the intermediate position, form only six almost equal bond lengths with O.

For simplicity, if we assimilate the incommensurate component of the modulation vector to the nearest rational value ($\frac{1}{7}$), we can describe the arrangement of the hexagonal tunnel with a regular sequence of seven subcells (Fig. 7). The first six are occupied by Ba atoms at the sites Ba1, Ba1, Ba3, Ba3, Ba2 and Ba2, respectively. The seventh cell is occupied by a Ca atom or eventually by a vacancy located at the site Ba3.

This sequence has the advantage of avoiding the eventuality of two contiguous cells where two Ba atoms occupy Ba1 and Ba2 sites, giving rise to too short Ba2—Ba1 distances (Ba2—Ba1 $\simeq$ 1.7 Å). Moreover, the presence of a vacancy or of a Ca atom at the end of the sequence generates a relaxation of the wall of the hexagonal tunnel and a consequent displacive modulation of the O atoms defining the wall of the hexagonal tunnel. As can be observed on the plots of the evolution of the Ba—O and O—O distances in Figs. 12 and 13, where the vacancy or the Ca substitution takes place, Ba—O distances of $\sim$ 2.4 Å are observed and the shorter O—O distances are encountered in the hexagonal tunnel (Fig. 13). The observed value of 2.4 Å is much too short for Ba—O bonds, but is in very good accordance if the Ba atom is substituted by Ca. We can definitely conclude that a substitution between Ca and Ba occurs in the hexagonal tunnel. The chemical formula proposed by EDX analysis is in very good agreement with the existence of a Ca atom every seven atoms in the hexagonal tunnels, as suggested by the refinement of powder diffraction data.

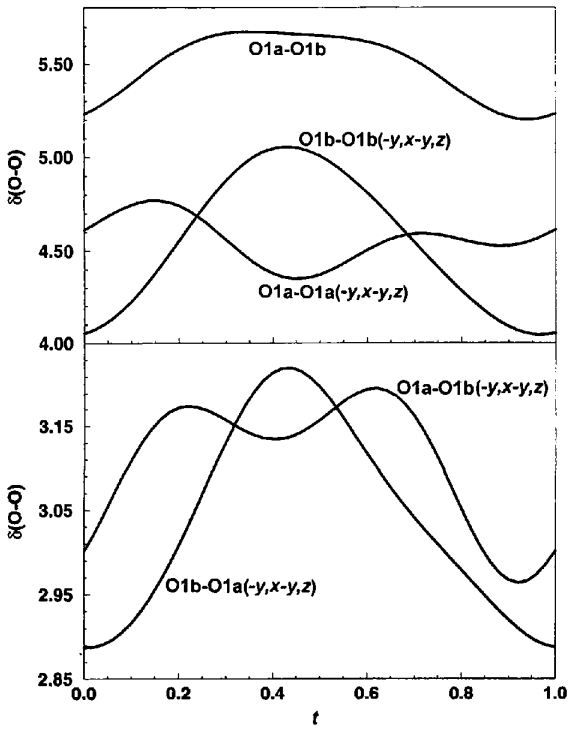

Fig. 13. O—O distances showing the shrinkage of the hexagonal tunnel where the Ca substitution occurs.

The remainder of the structure is concerned with very small modulated displacements. The Ca—O bond lengths are between 2.26 and 2.48 Å, while In—O bond lengths are between 2.02 and 2.38 Å. O—O distances of the In octahedron range between 2.89 and 3.22 Å.

The refinement of the modulated structure of $Ba_{0.85}Ca_{2.15}In_6O_{12}$ can be compared with the results of the study performed by Lalla *et al.* (1988). The atomic positions of the average structure are in good agreement with the single crystal determination. The temperature factors now have reasonable values and the high refined values in the refinement of Lalla *et al.* (1988) or in the present refinement of the average structure are consistent with the modulated disorder and with the modulated displacements determined in the refinement of the incommensurate structure (occupancy disorder of Ba atoms along the hexagonal tunnel axis, displacement of O1 along y and of O2 along z).

Other structures consisting of double octahedral chains exhibit a modulation of occupancy that affects the cations in the tunnel. The hollandite-related compound $La_{1.16}Mo_8O_{16}$ (Leligny, Labbé, Ledésert, Raveau, Valdez & McCarroll, 1992) consists of rutile chains sharing their edges and the corners of MoO_6 octahedra and forming large square tunnels, where La cations are located. In this structure occupational modulated pairs of La atoms occur in the square tunnel. The distance between the two atoms constituting the pair is also modulated. As in the structure of $Ba_{0.85}Ca_{2.15}In_6O_{12}$, the occupational modulation of the cations gives rise to a displacive modulation of the O atoms constituting the tunnel.

We can safely suggest that the incommensurate behavior observed in $Ba_{0.85}Ca_{2.15}In_6O_{12}$ arises from an attempt to provide the most stable environment for Ba atoms. As this configuration cannot be achieved within the average structure, a modulated phase takes place. This result shows that the tunnels in this type of structure are not very rigid and that it is possible to produce a significant expansion or shrinkage of the hexagonal tunnels. The incommensurate character of this phase can be characteristic of all the family of compounds exhibiting this type of average structure. It may be reasonable that phenomena such as the onset of the composite intergrowth structure may be common for this type of compound, presenting an almost continuous distribution of cationic sites along the tunnel axis. Nevertheless, in the present case, it was not possible to describe a specific Ba lattice and Ba atoms adapt the periodicity of their host tunnel *via* a modulated disorder over three distinct sites.

This work was supported by the European Community (Human Capital and Mobility Program). We are greatfully indebted to Dr J.-F. Bérar for the valuable modifications of the refinement program *XND* and to Dr Ph. Sciau for his assistance in X-ray powder data collection.

References

Bérar, J.-F. (1992). *APD 2nd Conference*. Gaithersburg, USA: NIST.

Bertaut, E. F., Blum, P. & Magnano, G. (1956). *Bull. Soc. Fr. Minéral. Cristallogr.* **129**, 536–561.

Cruickshank, D. M. J. (1964). *J. Inorg. Nucl. Chem.* **26**, 937–941.

Goutenoire, F., Caignaert, V., Hervieu, M., Michel, C. & Raveau, B. (1995*a*). *J. Solid State Chem.* **114**, 428–434.

Goutenoire, F., Caignaert, V., Hervieu, M., Michel, C. & Raveau, B. (1995*b*). *J. Solid State Chem.* **115**, 508–513.

Hill, P. M., Peiser, H. S. & Rait, J. R. (1956). *Acta Cryst.* **9** 981–986.

Lalla, A. & Müller-Buschbaum, Hk. (1988), *Z. Anorg. Allg. Chem.* **563**, 11–15.

Leligny, H., Labbé, Ph., Ledésert, M., Raveau, B., Valdez, C. & McCarroll, W. H. (1992). *Acta Cryst.* B**48**, 134–144.

Michel, C., Hervieu, M., Caignaert, V. & Raveau, B. (1992). *Acta Cryst.* C**48**, 1747–1749.

Petříček, V. (1994). *JANA94. Programs for Modulated and Composite Crystals*. Institute of Physics, Praha, Czech Republic.

Schenck, R. von & Müller-Buschbaum, Hk. (1973). *Z. Naturforsch.* **398**, 24–30.

Wilson, A. J. C. (1992). *International Tables for Crystallography*, Vol. C, pp. 384–391. Dordrecht: Kluwer Academic Publishers.

Wolff, P. M. de (1977). *Acta Cryst.* A**33**, 493–497.

Wolff, P. M. de, Janssen, T. & Janner, A. (1981). *Acta Cryst.* A**37**, 625–636.